3-D Acoustic Imaging of Broadband SAS data

Jim Christoff, JoEllen Wilbur and Dan Cook
Science Technology and Analysis Dept.
Coastal Systems Station, Dahlgren Division
Naval Surface Warfare Center
6703 Highway 98
Panama City, FL 32407-7001

Abstract - The difficult conditions encountered in the littoral region require development of flexible sonar processing technologies. One technical approach to increase the flexibility of active sonar has been the development of broadband sonar for multifrequency analysis. Physics based target models of acoustic backscatter use frequency as a prime variable, often defined in terms of radius, *a*, and acoustic wavenumber, *k*. For example, fluid filled spheres insonified at low frequencies exhibit sharp peaks and nulls in the acoustic backscatter. As *ka* increases marine biologists have predicted and observed a frequency variation in target strength associated with shape in the acoustic return of biologics that conform to fluid filled and elastic object models. The broadband synthetic aperture sonar (BBSAS) at CSS enables one to add another dimension (frequency) to the target feature space without compromising resolution. The processing enables a user to construct a 3-D image description around targets of interest. A modified STFT, Choi-Williams, and Binomial transformations, are compared for the frequency decomposition stage of the beamformer. A trade-off between processing complexity and preservation of the target characteristics is discussed.

I. INTRODUCTION

The target response to an incident broadband waveform is the superposition of an aspect dependent specular response and an aspect independent free oscillation period [1]. The early-time response is referred to as the specular response from the surface as the incident pulse traverses the target. The late-time response, or free oscillation period, is due to energy deposited into the target and contains the natural frequencies of the target [2,3]. The late-time response of the target is said to be aspect independent in that the locations of the associated poles in the complex frequency plane does not change with target orientation. The associated strength of each natural frequency is however a function of aspect. That is, each natural frequency of the target has a characteristic beampattern associated with it and the collection of frequency bands represents the target response.

Application of time-frequency concepts to the acoustic response from elastic targets has been well established [4]. Several papers have explored the potential merits of an expanded target description and purported time-frequency concepts to offer a robust feature set for target classification [2,4,5,6,7,8]. Yet, very little has appeared in the literature to address the integration of these concepts into a practical system. Pinto, Belletini, Hollett and Tesei [9] observed the echo response from a spherical shell in the spectrogram of the maximum target response of beamformed data.

This paper examines issues involved with integrating a frequency-dependent characterization into a practical sonar imaging system. Section II briefly overviews several common time-frequency transformations used to represent acoustic targets. Section III discusses target volume description first from controlled tank data then SAS data collected during sea tests.

II. DISCUSSION

A. Time-frequency mappings

This section overviews four common time-frequency mappings: the Wigner distribution, the Choi-Williams, the binomial transform and the short-time-Fourier transform. The discussion in this section is brief as most of the underlying theory for these transformations can be found in the literature [10]. The focus of this paper is concept integration into a system.

The spectrogram is still the most common technique for observing the time-evolutionary nature of the signal spectrum. The spectrogram is calculated using a short-time Fourier transform (STFT) analysis within a moving window. The trade-off between resolution in time versus frequency is well known [10].

The Wigner distribution serves as a baseline for time-frequency representations of continuous, aperiodic, harmonizable functions whose marginal domains are related through the Fourier transform. The class of related time-frequency distributions is referred to as the Cohen class [10]. The STFT fits into this class as a smoothed member of the Wigner distribution. The Wigner distribution is the only bilinear t-f distribution in the Cohen class which is simultaneously covariant to time and frequency

0-933957-31-9

Report Documentation Page

Form Approved
OMB No. 0704-0188

Public reporting burden for the collection of information is estimated to average 1 hour per response, including the time for reviewing instructions, searching existing data sources, gathering and maintaining the data needed, and completing and reviewing the collection of information. Send comments regarding this burden estimate or any other aspect of this collection of information, including suggestions for reducing this burden, to Washington Headquarters Services, Directorate for Information Operations and Reports, 1215 Jefferson Davis Highway, Suite 1204, Arlington VA 22202-4302. Respondents should be aware that notwithstanding any other provision of law, no person shall be subject to a penalty for failing to comply with a collection of information if it does not display a currently valid OMB control number.

1. REPORT DATE **01 SEP 2003**	2. REPORT TYPE **N/A**	3. DATES COVERED
4. TITLE AND SUBTITLE **3-D Acoustic Imaging of Broadband SAS data**		5a. CONTRACT NUMBER
		5b. GRANT NUMBER
		5c. PROGRAM ELEMENT NUMBER
6. AUTHOR(S)		5d. PROJECT NUMBER
		5e. TASK NUMBER
		5f. WORK UNIT NUMBER
7. PERFORMING ORGANIZATION NAME(S) AND ADDRESS(ES) **Science Technology and Analysis Dept. Coastal Systems Station, Dahlgren Division Naval Surface Warfare Center 6703 Highway 98 Panama City, FL 32407-7001**		8. PERFORMING ORGANIZATION REPORT NUMBER
9. SPONSORING/MONITORING AGENCY NAME(S) AND ADDRESS(ES)		10. SPONSOR/MONITOR'S ACRONYM(S)
		11. SPONSOR/MONITOR'S REPORT NUMBER(S)
12. DISTRIBUTION/AVAILABILITY STATEMENT **Approved for public release, distribution unlimited.**		
13. SUPPLEMENTARY NOTES		
14. ABSTRACT		
15. SUBJECT TERMS		

16. SECURITY CLASSIFICATION OF:			17. LIMITATION OF ABSTRACT	18. NUMBER OF PAGES	19a. NAME OF RESPONSIBLE PERSON
a. REPORT **unclassified**	b. ABSTRACT **unclassified**	c. THIS PAGE **unclassified**	**UU**	**7**	

translation of the signal and for which the time-reversal property and Moyal's formula are satisfied [11].

The most noted disadvantage to the WD is the generation of cross-terms associated with the bilinear nature of the mapping. Several derivatives of the WD have been developed to attenuate these additional artifacts. Smoothing operations on the WD reduce cross-terms but at the cost of finite support, among other properties [12]. An early attempt to reduce cross-terms with a kernel operation integrated into the WD computation was the Choi-Williams or energy distribution (ED)[13]. The performance of the Choi-Williams has been compared extensively to that of the WD and the STFT over a number of applications and the ED has become a baseline for examining other reduced interference time-frequency mappings [10].

An entire class of time-frequency distributions has evolved which attenuate undesirable artifacts through integration of a kernel function into the WD computation. These are referred to as reduced-interference distributions (RID). The designs of appropriate kernel functions for various applications have been extensively studied. The binomial transform is one such RID that has been found to be particularly well suited to digital data [9,10]. An overview of these concepts can be found in [10 ch3].

B. Mapping Sampled Data

Although often overlooked, data sampling is key to the application of t-f to the broadband SAS. In fact, it has been demonstrated that the response to cross-term attenuation between the target eigenfrequencies in the discrete t-f computations cannot and should not be treated as sampled versions of the continuous case [11]. Because the focus here is integration of t-f concepts into a broadband SAS the discussion below concentrates specifically to t-f mapping of data sampled at or near the Nyquist rate.

The following notation is used in the discussion:

$$\left\langle f \,\middle|\, x \right\rangle_M \equiv \sum_{i=0}^{M-1} f_i x_i \tag{1.1}$$

$$f(m) \underset{m}{*} x(m) = \sum_{m=0}^{M-1} \left\langle f_i \,\middle|\, x_{m-i} \right\rangle \delta\left(t - \frac{m}{f_s}\right) \tag{1.2}$$

$$F_k = \left\langle f_m \,\middle|\, e^{-j\frac{2\pi mk}{M}} \right\rangle_M \equiv DFT \tag{1.3}$$

The data vector defines the sampled target impulse response

$$f(m) = \sum_{m=0}^{M-1} f_m \delta\left(t - \frac{m}{f_s}\right) \tag{2}$$

where f_s is the sampling frequency and δ is the Delta functional. The discrete-WD (DWD) of the sampled target impulse response function, *f(m)*, is calculated by first upsampling the data by a factor of 2, forming the local autocorrelation matrix, **R**, with matrix elements

$$R_{m,i} = f_{m+i} f_{m-i}^{*} \tag{3}$$

then taking the DFT of **R** across column vectors to form the matrix elements for the t-f DWD**.** Both the DWD and the discrete form of the Choi-Williams (or the discrete-windowed ED) require upsampling of the data. It has been pointed out that for Nyquist sampled signals, f_{N_s}, interpolation is not required in the DWD and DWED for analytic signals. However, the broadband SAS data is already sampled to, $f_{N_s}/2$, to account for the analytic signal so upsampling is required. The STFT and the BTRID do not require data interpolation.

The DWD data matrix, **W**, is defined by the elements

$$W_{m,k} = \left\langle R_{m,i} \,\middle|\, e^{-j\frac{2\pi ik}{M}} \right\rangle_M . \tag{4}$$

In its digitized form the Choi-Williams, or ED, can only be approximated. A digitized approximation to the windowed-ED [10 ch7] is calculated as

$$C_{m,k} = \left\langle R(m,i) \underset{m}{*} G(m,i) \middle/ \left\langle G_{m,i} \right\rangle_M \,\middle|\, e^{-j\frac{2\pi ik}{M}} \right\rangle_M \tag{5.1}$$

where

$$G_{ED}(m,i) \cong \frac{\sqrt{\sigma/2\pi}}{2i} e^{-\frac{\sigma m^2}{4i^2}} . \tag{5.2}$$

A particularly convenient discrete RID kernel is the taken from the binomial distribution. The BTRID has been shown to be particularly well suited to acoustic signal descriptions for applications where oversampling of the data is not practical [9]. The BTRID is calculated from (5.1) but with the kernel operation derived from the binomial distribution as

$$G_B(m,i) = \frac{1}{2^{|i|}} \sum_{n=0}^{|i|} \binom{|m|}{n} \delta(m + \tfrac{|i|}{2} - n)\,. \tag{5.3}$$

The Z-transform of (5.3) taken in *m* yields

$$g_B(z,i) = \left(\frac{z + z^{-1}}{2} \right)^{|m|} \tag{6}$$

enabling a filter realization of the convolution defined in (5.1) [10 ch3].

The short-time-Fourier transform (STFT) is still the fastest and most common digital t-f transformation. The STFT data matrix, **S**, is created from the matrix elements

$$S_{m,k} = \left\langle f_i h_{m-i} \middle| e^{-j\frac{2\pi i k}{M}} \right\rangle_M . \tag{7}$$

The spectrogram is derived from the magnitude squared of the STFT. Although not computed this way, the STFT can be interpreted as a smoothed DWD where the DWD is convolved in both *m* and *k* directions. Using this interpretation the sliding window function, *h(m)*, can be designed to optimize the resultant t-f output of the STFT. By definition a window that assumes the form of the exponent of a quadratic (e.g. Gaussian) gives minimum signal spreading in the t-f plane of the STFT. The choice for the smoothing factor for the Gaussian window is controlled by the application. Under this interpretation a more flexible form of the Gaussian windowed STFT (GWSTFT) is the smoothed-DWD (SDWD) where the local autocorrelation matrix is substituted by

$$R_{m,i} = \sum_{n=-M_h/2}^{M_h/2} h_n h_{-n}^{*} f_{m+i+n} f_{m-i+n}^{*} . \tag{8}$$

The SDWD with a Gaussian window does not maintain as many signal properties as the DWED and BTRID, however is it computationally much simpler for attenuating cross-terms. Because the DWD is calculated, upsampling is required.

Sessarego, Sageloli, Flandrin, and Zakharia [4], among others, have used various forms of the Wigner representation for a time-frequency characterization of the acoustical scattering from a spherical shell. In their analysis they observed velocity dispersion of certain surface waves. Subsequent time-scale analyses of the scattering from spherical shells have produced similar observations [7]. Each of these studies involved highly oversampled data.

Figures 1(a-f) illustrate the various t-f mappings using the backscatter model for a 2% spherical shell. What differs here from most analysis is the target impulse response data is sampled at only 1.5 times the Nyquist rate for analytic data. This form of sampling rate is more in line with SAS data.

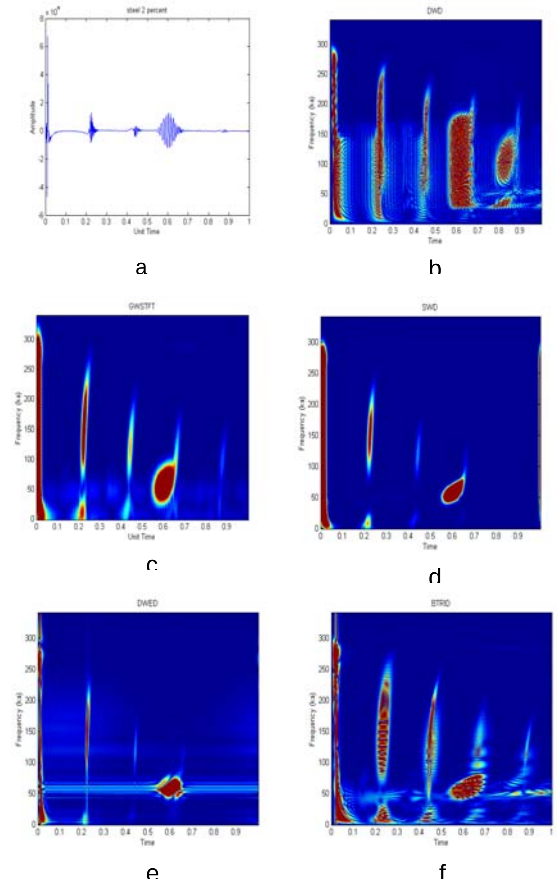

Fig. 2. Response characterizations from a 2% spherical shell. (a) Sampled impulse response. The remaining are magnitude plots of the time-frequency calculated using the (b) discrete Wigner distribution (c) Gaussian-windowed STFT (d) smoothed-discrete Wigner distribution (e) discrete-windowed energy distribution (Choi-Williams approximation) (f) binomial transform reduced interference distribution.

Figure 1a gives the sampled impulse response from the sphere. A discussion of the various modes seen in the response function can be found in [1,2,4,5]. Figures 1(b-f) give the magnitude plots for the respective DWD, GWSTFT, SDWD, DWED and BTRID. As expected, the DWD maintains cross-terms leaving visualization difficult. If visualization is unimportant however, a target volume created from the DWD enables the creation of meaningful feature vectors. The DWED was robust on highly sampled data however for the lower sampling rate the DWED degrades considerably. The SDWD is visually appealing but its computation is considerably more intense than the GWSTFT for only a moderate gain in resolution. The BTRID is able to resolve individual frequencies within each time bin better than any of the other t-f mappings pictured. The BTRID maintains the desirable properties associated with RID t-f mappings [10 ch3]. The BTRID provides a t-f

mapping for highly resolved visualization and the creation of feature vectors in the study of target characteristics.

The GWSTFT is the fastest and simplest mapping to compute. The GWSTFT maintains the scaling relationship between pings in a data matrix. The GWSTFT is more flexible, can serve as a filterbank and in its complex form can be applied at any stage in the SAS processing. For an N pings by M samples data set, integration of the GWSTFT data across k reproduces the original data matrix.

III. DATA ANALYSIS

In this section the GWSTFT is used to generate a target volume description from data collected from a free field target suspended in a fluid filled tank. Next the GWSTFT is applied to the broadband SAS to create a frequency dependent image series.

A. Target Description Using Tank Data

Broadband linear FM acoustic backscatter data was collected during tests conducted in ARL/UT's sand tank. Each data file is sampled over an interval that is large relative to the echo duration with sufficient sampling both prior to the echo onset and post echo return to enable meaningful target characterization. Data collected over 360 degrees in 2-degree increments is processed to generate a descriptive target pattern. The data is pulse compressed and system artifacts are removed using adjacent channels over the entire frequency band.

The waveform samples are related to the target transfer function through a sampled convolution of the form

$$y_m^n = \int_{-\infty}^{\infty} (\hat{f}^n(t) \underset{t}{*} x(t))\delta(t - \frac{m}{f_s})dt \qquad (9)$$

where *x(t)* denotes the transmit waveform and $\hat{f}(t)$ is the system corrupted impulse response function of the target for an angle of incidence corresponding to *n*. Inverse filtering of the data yields $\hat{f}(t) \to f(t)$.

The sampled estimate of the target impulse response function over N pings forms the data matrix $\mathbf{f}=(f^1(m)\ f^2(m)\ \ldots\ f^N(m))$, calculated as

$$f^n(m) = \sum_{m=0}^{M_f-1} \frac{1}{M_f} \left\langle F_k^n \middle| e^{-j\frac{2\pi mk}{M_f}} \right\rangle_{M_f} \delta(t - \frac{m}{f_s}) \qquad (10.1)$$

where

$$F_k = \frac{X_k^* Y_k}{X_k^* X_k + \alpha |X_k|_{\max}^2} \qquad (10.2)$$

for F_k, X_k and Y_k the respective DFT coefficients of *f(m)*, *x(m)* and *y(m)* and α is set to keep the deconvolution operation within the receiver passband [14]. The processed data matrix defined by **f** is then applied to the time-frequency transformation mappings defined in Section II to create the target volume description.

The 3-dimensional scaled target volume characterization is a function of time-frequency-aspect. Integration of the squared magnitude along the time axis (extent) yields target strength as a function of frequency and aspect angle. The volume graphics employs a 256 scale with background normalization to 64 and clipping at 255. Scattered returns from a broadside incident angle considerably dominate the response then attenuate rapidly as the incident waveform moves off axis.

Figures 2(a-c) illustrate the t-f target response by graphing slices at different incident aspect angles through the volume generated using the GWSTFT. Fig. 2a gives slices through the volume for the broadside response of the target before clipping. Characteristic information from slices taken through the volume at broadside post clipping would not be robust in frequency unless normalization is performed independently for each look. Notice from the slice planes illustrated in Fig. 2b that although the amplitudes vary with aspect the dominant frequency bands of the target are independent of aspect. Fig. 2d plots slice planes taken through the volume at selected frequency bands.

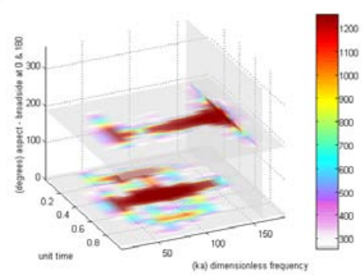

(a)

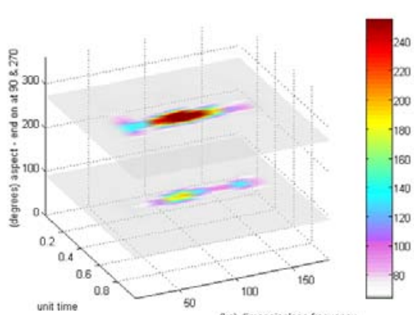

(b)

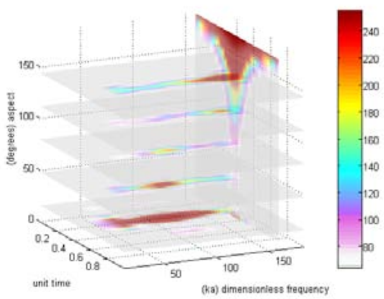

(c)

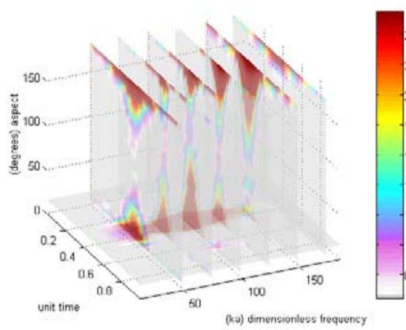

(d)

Fig. 2. Target volume slice planes through the target volume generated using the GWSTFT. (a) Slice planes at broadside prior to clipping. Target strength is very high at broadside and clipping removes frequency dependence. TS attenuates rapidly as the aspect moves off broadside. (b) Slice planes at target ends. (c) Slice planes off axis. Notice the regions of strongest frequency do not change with aspect, only the amplitudes change. (d) Slice planes orthogonal to the t-f plane.

Fig. 3a gives relative non-dimensional TS as a function of ka and aspect obtained by integration along the unit time axis. Actual target strengths are not needed to illustrate the concept. Fig. 3b is after ping-by-ping normalization. Figures 3(a-b) taken together demonstrate that the weights of the target eigenfrequencies are indeed aspect dependent while the location of the target eigenfrequencies in the Z-transform are in fact aspect independent. This agrees with acoustic scattering theory [1,2].

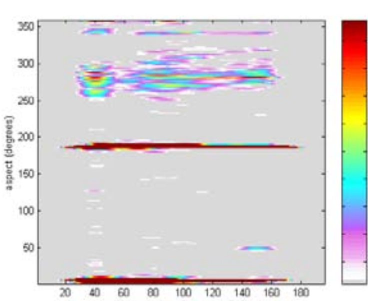

(a)

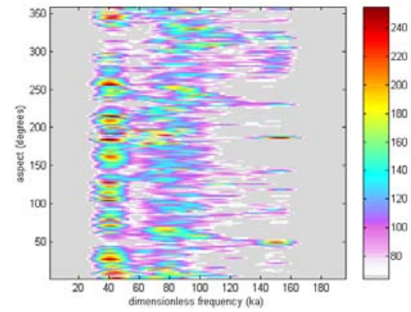

(b)

Fig. 3. Non-dimensional target strength as a function of dimensionless frequency ka and aspect angle of incident waveform. (a) Derived from target volume. (b) Result from volume with ping-by-ping normalization to illustrate frequency band consistency.

B. SAS Data

The final set of examples illustrate the application of the GWSTFT with a 40 microsecond Gaussian window to Broadband SAS data collected in the Gulf of Mexico, Panama City, FL in September of 2001. The Coastal Systems Station (CSS) synthetic aperture sonar (SAS) is a side-scan sonar that forms a high-resolution image by coherently combining multiple pings [15]. The CSS HF/LFSAS is a dual frequency sonar capable of creating both high and low frequency images. The high frequency narrowband mode produces high-resolution images to depict target highlights and shadow for classification. The low frequency mode includes a broadband projector with an operational mode from 8-55kHz. The broadband mode captures frequency dependent characteristics of the target. Combined, the HF/LFSAS is capable of producing a robust feature set for classification. The BBSAS data depicted here refers to the broadband low frequency mode.

The BBSAS first creates an image over a large viewing area for the complete band. The user then defines a rectangular region of interest by moving the mouse over the image and clicking the upper and lower corners to create a boxed area for further viewing. A volume description of the boxed area is then created.

Figures 4(a-c) plot the target volume for a boxed region around a target of interest. The same volume is illustrated over different viewing angles. The visualization of the target volume is created from frequency slice plane images of 5 kHz frequency sub-bands. Fig. 4a gives the same viewing angle depicted in the previous target examples. Fig. 4b gives a viewing angle looking down on the volume from the

top to examine the frequency and extent of the target in the range direction. Fig. 4c gives the view looking along the direction of the frequency vector into the x-y slice planes.

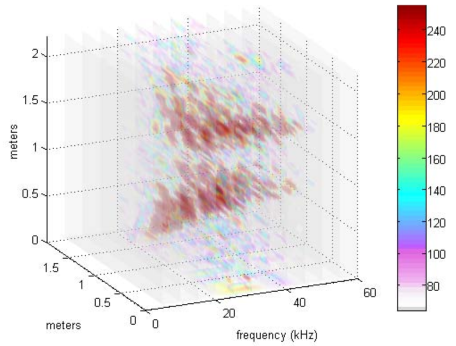

(a)

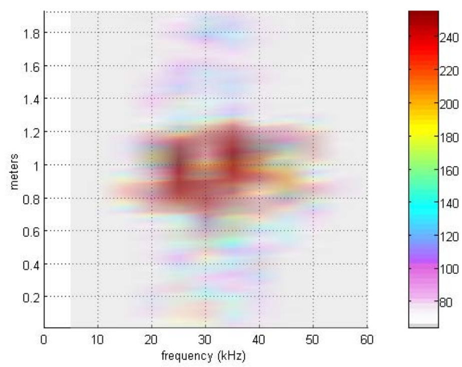

(b)

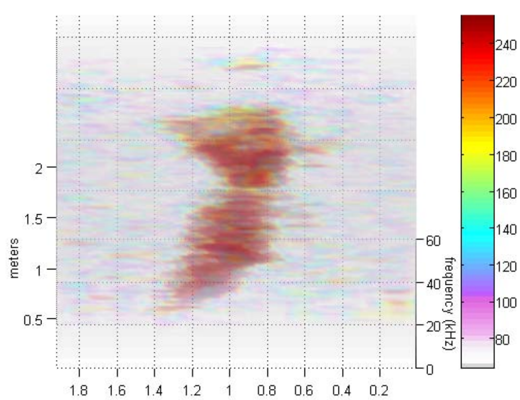

(c)

Fig. 4. Volume slice planes through SAS target volume generated from GWSTFT for 5kHz frequency bin widths. Different view angles indicated by view = (azimuth, elevation). (a) View angle = (-37.5,30). (b) View looking down from the top (0,90) . (c) View of (x,y) looking orthogonal to the frequency slice planes (90,0).

IV. SUMMARY

The application of frequency distribution mappings for acoustic characterization of submerged elastic targets was examined. The impact of working with Nyquist and near Nyquist sampled data matrices over multiple pings was detailed. The GWSTFT mapping was applied to response data from a free field target collected in controlled tank tests to study the utility of a multi-frequency target volume description. The target volume description was found to agree with acoustic theory. The GWSTFT mapping was then applied to the BBSAS beamformer for the generation of a target volume description within a user-defined region around targets of interest.

REFERENCES

[1] *Acoustic Resonance Scattering*, ed. H. Uberall, (Gorden and Breach Science Pub., Philadelphia, PA, 1992).

[2] J. Wilbur and N.P. Baum, “Acoustic Singularity Identification,” in *Detection and Identification of Visually Obscured Targets*, ed. C.E. Baum, (Taylor and Francis, Washington DC, 1996), Chap. 10.

[3] J. McCorkle, V. Sabio, R. Kapoor, and N. Nandhakumar, “Transient Synthetic Aperture Radar and the Extraction of Anisotropic and Natural Frequency Information,” in *Detection and Identification of Visually Obscured Targets*, ed. C.E. Baum, (Taylor and Francis, Washington DC, 1996), Chap. 12.

[4] J.P. Sessarago, J. Segaloli, P. Flandrin, and M. Zakharia, “Time-Frequency Analysis of Signals Related to Scattering Problems in Acoustics. Part I: Wigner-Ville Analysis of Echoes Scattered by a Spherical Shell,” in *Wavelets: Time Frequency Methods and Phase Space*, ed. J.M. Combes, A. Grossmann, and Ph. Tchamitchian, (Springer-Verlag, NY, 1988), pp.147-153.

[5] J. Wilbur and R. J. McDonald, “Resonant Pole Identification from the Acoustic Backscatter of Small Submerged Multi-specular Elastic Targets,” *Proc. IEEE Int. Conf. Acoust., Speech and Sig. Process.*, May 1996, Atlanta, GA, Vol. SSAP

[6] J. Wilbur and S. G. Kargl, “Application of Wavelets to Acoustic Resonance -- Elastic Targets Surrounded by Biologics,” *Proc. IEEE Int. Conf. Acoust., Speech and Sig. Process.,* Apr. 1993, Minneapolis, MN, Vol. IV, pp. 492-495.

[7] C. Baudet, O. Michel, and W. Williams, “Detection of coherent structures using time-scale resolved acoustic spectroscopy,” arXiv:chao-dyn/9804010 v2, Nov. 1998.

[8] M. Till and S. Rudolph, "Optimized time-frequency distribution for acoustic signal classification," *Proc. SPIE*, VIII, Orlando, FL, April 2001.
[9] M. Pinto, A. Bellettini, R. Hollett, and A. Tesei, "Real- and Synthetic-Array Signal Processing of Buried Targets," *IEEE J. Oceanic Engineering*, vol. 27, no. 3, July 2002, pp. 484-494.
[10] *Time-Frequency Signal Analysis*, ed. B. Boashash, (Wiley Press, Australia, 1992).
[11] J. O'Neill and W. Williams, "Distributions in the Discrete Cohen's Classes," *IEEE Int. Conf. On Acoust., Speech and Sig. Process.,* vol. 3, no. 1062, pp. 1581-1584.
[12] W. Martin and P. Flandrin, "Wigner-Ville Spectral Analysis of Nonstationary Processes," *IEEE Trans. Acoust., Speech and Sig. Process.,* vol 33., pp. 1461-1470, 1985.
[13] H. Choi and W. Williams, ""Improved Time-Frequency Representation of Multi-component Signals Using Exponential Kernels," *IEEE Trans. Acoust., Speech, Sig. Process.,* vol. 37, no. 6, pp. 862-871, 1989.
[14] G. J. Dobeck, "Optimal Matched Filters," *CSS Signal Processing Seminar Series*, Nov. 1995
[15] G. Sammelmann, J. Fernandez, J. Christoff, L. Vaizer, J. Lathrop, R. Sheriff, and T. Montgomery, "High frequency/low frequency synthetic aperture sonar," *Proc. SPIE*, vol. 3079, pp. 160-171, 1997.
[16] J. Christoff, D. Cook, A. Davenport, J. Fernandez, and J. Piper, "Low Frequency/High Frequency Synthetic Aperture Sonar," CSS Technical Report, in press.